Modern Physics Letters B
Vol. 35, No. 21 (2021) 2150357 (11 pages)

DOI: 10.1142/S0217984921503577

World Scientific
www.worldscientific.com

Metal–insulator transitions of fermionic mixtures with mass imbalance in disordered optical lattice

Anh-Tuan Hoang* and Thi-Hai-Yen Nguyen†

Institute of Physics, Vietnam Academy of Science and Technology, Hanoi, Vietnam
Graduate University of Science and Technology, Vietnam Academy of Science and Technology, Hanoi, Vietnam
**hatuan@iop.vast.ac.vn*
†*nhyen@iop.vast.ac.vn*

Duc-Anh Le

Faculty of Physics, Hanoi National University of Education, Xuan Thuy 136, Cau Giay, Hanoi 10000, Vietnam
anhld@hnue.edu.vn

Received 1 July 2020
Revised 29 March 2021
Accepted 19 April 2021
Published 9 June 2021

We study the metal–insulator transitions in the half-filled Anderson–Hubbard model with mass imbalance by the typical medium theory using the equation of motion method as an impurity solver. The nonmagnetic ground state phase diagram of the system with mass imbalance is constructed numerically. In addition to the three phases showed up in the balanced case, the phase diagram of the mass imbalanced case contains a spin-selective localized phase, where one spin component is metallic while the other spin component is insulating. We find that if one increases the mass imbalance the metal region in the phase diagram is reduced, while both Anderson and Mott insulator regions are enlarged.

Keywords: Metal–insulator transitions; Anderson–Hubbard model with mass imbalance; typical medium theory.

1. Introduction

The recently developed experiments with ultracold atoms in optical lattices have provided very promising tools to investigate the fields of interacting and disordered systems in condensed matter physics. Compared to condensed matter systems, the ultracold gases give numerous advantages such as high degree of control and tunability. In particular, the interaction between atoms has been controlled by

*Corresponding author.

means of the Feshbach resonance,[1,2] and the dipolar force may be used to simulate disordered optical potential, as a result the Anderson–Hubbard model (AHM) can be designed.[3] In addition, the spin SU(2) symmetry of the system can be broken by coupling to an external magnetic field[4] or by using two atom species with different masses.[5,6] This leads to different hopping parameters $t_\uparrow$ and $t_\downarrow$ in AHM and enables one to set up the mass imbalanced AHM, which is defined as

$$H = \sum_{\langle i,j\rangle,\sigma} t_\sigma (a^+_{i\sigma} a_{j\sigma} + \text{h.c.}) + \sum_{i,\sigma} (\varepsilon_i - \mu_\sigma) n_{i\sigma} + U \sum_i n_{i\uparrow} n_{i\downarrow}, \tag{1}$$

where $a_{i\sigma}(a^+_{i\sigma})$ annihilates (creates) a fermion with spin σ at site i, $n_{i\sigma} = a^+_{i\sigma} a_{i\sigma}$ is the particle operator, U is the on-site Coulomb interaction, t_σ and μ_σ are the nearest-neighbor hopping parameter and the chemical potential for the fermion with spin σ, respectively. The ionic energy ε_i is a random variable, describing the local disorder disturbing a motion of mobile particles. In our problem, we assume a box distribution for the ionic energies ε_i: $P(\varepsilon_i) = \Theta(\Delta/2 - |\varepsilon_i|)/\Delta$, where Θ is the Heaviside step function and Δ is the disorder strength. The mass imbalance parameter is defined as $r = t_\downarrow/t_\uparrow$ with two limits: $r = 0$ corresponding to the Anderson–Falicov–Kimball model (AFKM) and $r = 1$ to the AHM.

It should be noted that the mass imbalance strongly affects the Mott metal–insulator transition (MIT) in the Hubbard model (HM), for example, both spin components localize simultaneously at the critical value of the on-site Coulomb interaction, which decreases monotonically as increasing the mass imbalance.[7–10] In comparison with phase diagram of the HM, that of the AHM is richer and more attracting because of the appearance of the Anderson localization besides the Mott one. Therefore, it would be interesting to investigate how the mass imbalance affects the Mott and Anderson localization in the AHM. However, the AHM is rather difficult to deal with compare to the HM, and one thus has to proceed some approximations.

The dynamical mean field theory (DMFT) with geometrical average over the disorder [it is also known as the typical medium theory (TMT)] providing an explicit criterion for Anderson localization has proven to be a successful method to investigate the physics of strongly correlated fermion on a disordered lattice. In this non-perturbative approach the typical density of states (TDOSs) is calculated by taking the geometrical averaging of the local density of state (LDOS) over the disorder configurations and is used as an order parameter for Anderson localization transition.[11–16] The TMT has been employed to study the MIT in AFKM[12] as well as in AHM[13,16,17] and in the disorder charge-transfer model.[18] Notably, the non-magnetic phase diagrams of the half-filled AFKM and AHM are similar: the two insulating phases (Mott and Anderson insulators) surrounded by the correlated metal. However the metal region in the AFKM is significantly smaller than those in the AHM.[12,17] Recently, this method has been used by Skolimowski *et al.* to calculate the electronic and magnetic phase diagrams of the AHM at half-filling with spin-dependent diagonal disorder.[19,20] Besides the Mott insulator, the Anderson

localization, and correlated disordered metallic phase, they found a new state, where the spin-up particles are localized while those with spin-down are still itinerant and referred to it as spin-selective localized phase.[19,20] The latter is possible because the particle-hole and SU(2) spin symmetries are broken via spin-dependent diagonal disorder so that the particles with spin-up move on a lattice with a random potential whereas the particles with spin-down propagate on a uniform lattice.[19,20] However, the existence of spin-selective localized phase when the SU(2) spin symmetry is broken via other mean than spin-dependent diagonal disorder while the particle-hole symmetry is still preserved remains unclear.

In this report, the DMFT using the equation of motion (EOM) method as an impurity solver with geometrical average over the disorder configurations are used to study the paramagnetic ground state in the mass imbalanced AHM at half-filling. Within the DMFT, the many-body lattice problem is mapped onto a local impurity model. While the lattice problem is in general intractable, the impurity model is usually solvable through various schemes such as the quantum Monte Carlo (QMC) method, the numerical renormalization group (NRG), the iterated perturbation theory (IPT), the exact diagonalization (ED) method, and the EOM method. However, each impurity solver has its own limitation. For example, a major limitation of QMC (specially for fermions) is the sign problem at low temperature which depends on the basis used to rewriting the partition function. In addition, QMC has to work on the imaginary time which later will require an analytic continuation for the spectrum. The latter also applies for ED. NRG can give a good description of the low frequency quasiparticle peak associated with low-energy excitations, it has less precision in the Hubbard bands. Although QMC, NRG, and ED are numerically exact impurity solvers but they are computational expensive, with their application strongly limited by available computer resources. On the other hand, IPT and EOM are much more reliable when the computer resources are limited. In the IPT, one has to introduce an ansatz to interpolate the weak and strong coupling limits. Also, the IPT fails away from half-filling when the interaction strength is much larger than the bandwidth thus it is not always suitable. EOM are of course limited by their decoupling schemes, but EOM has shown its value by working directly on the real frequency axis and at very low temperature. It can be good candidate for a fast and reliable impurity solve by choosing a suitable decoupling scheme.[21] As noted in Ref. 16 in the balanced case, the phase diagram obtained by TMT-DMFT with the EOM is in fairly good agreement with those found from the statistical DMFT and the TMT-DMFT with the NRG and the SB4. Therefore, we will employ the EOM as the impurity solver. We found that with increasing the mass imbalance both Anderson and Mott insulator regions are enlarged. In addition, for the mass imbalance parameter $0 < r < 1$ a line of the spin-selective localized phase, where the spin-down particles are localized, while those with spin-up are still itinerant, appears.

2. Theoretical Formulation

The Hamiltonian model (1) is solved within the DMFT.[14,22] The effective single-impurity Anderson model with different ε_i reads

$$H_{\text{imp}} = \sum_{\sigma}(\varepsilon_i - \mu_\sigma)n_{i\sigma} + Un_{i\uparrow}n_{i\downarrow} + \sum_{k\sigma}\varepsilon_{k\sigma}c^{+}_{k\sigma}c_{k\sigma} + \sum_{k\sigma}(V_{k\sigma}c^{+}_{k\sigma}a_{i\sigma} + V^{*}_{k\sigma}a^{+}_{i\sigma}c_{k\sigma}). \quad (2)$$

Here, $c_{k\sigma}$ ($c^{+}_{k\sigma}$) denotes the annihilation (creation) operator of the bath fermions with spin σ. The hybridization matrix elements $V_{k\sigma}$ and the dispersion parameter $\varepsilon_{k\sigma}$ define the hybridization function as

$$\eta_\sigma(\omega) = \sum_k \frac{|V_{k\sigma}|^2}{\omega - \varepsilon_{k\sigma}}. \quad (3)$$

In order to study MIT in the system, for each ionic energy ε_i, we calculate the LDOSs $\rho_\sigma(\omega, \varepsilon_i) = -\Im G_\sigma(\omega, \varepsilon_i)/\pi$. From this, we obtain the geometrically averaged LDOS $\rho_{\sigma g}(\omega) = \exp[\langle \ln \rho_\sigma(\omega, \varepsilon_i)\rangle]$ as well as the arithmetically averaged LDOS $\rho_{\sigma a}(\omega) = \langle \rho_\sigma(\omega, \varepsilon_i)\rangle$, where $\langle O(\varepsilon_i)\rangle = \int d\varepsilon_i P(\varepsilon_i)O(\varepsilon_i)$ is an arithmetic mean of $O(\varepsilon_i)$. The real part of the lattice Green function is given by the Hilbert transformation

$$G_{\sigma\alpha}(\omega) = \int d\omega' \frac{\rho_{\sigma\alpha}(\omega')}{\omega - \omega'}, \quad (4)$$

where α stands for either "g" or "a".

We choose the non-interacting density of states (DOSs), $\rho^0_\sigma(z) = \frac{1}{2\pi t^2_\sigma}\sqrt{4t^2_\sigma - z^2}$, for which the local Green function and the hybridization function are related by

$$\eta_\sigma(\omega) = t^2_\sigma G_\sigma(\omega). \quad (5)$$

We now employ the equations of motion method[16,22] for solving the effective single-impurity Anderson model (2). For the paramagnetic case at half-filling: $\langle n_{i\uparrow}\rangle = \langle n_{i\downarrow}\rangle = \langle n_i\rangle/2$ and $\mu_\uparrow = \mu_\downarrow = U/2$. The local Green function in this case can be approximately expressed as

$$G_\sigma(\omega, \varepsilon_i) = \frac{1 - \langle n_i\rangle/2}{\omega - \varepsilon_i + U/2 - \eta_\sigma(\omega) + U\eta_{\bar\sigma}(\omega)[\omega - \varepsilon_i - U/2 - \eta_\sigma(\omega) - 2\eta_{\bar\sigma}(\omega)]^{-1}} \frac{\langle n_i\rangle/2}{\omega - \varepsilon_i - U/2 - \eta_\sigma(\omega) - U\eta_{\bar\sigma}(\omega)[\omega - \varepsilon_i + U/2 - \eta_\sigma(\omega) - 2\eta_{\bar\sigma}(\omega)]^{-1}}. \quad (6)$$

Equation (6) reproduces the result in AFKM[12] for $r = 0(t_\downarrow = 0)$ and in the mass-balanced AHM[16] for $r = 1(t_\uparrow = t_\downarrow)$. In the nondisorder limit, $\varepsilon_i = 0$, Eq. (6) is reduced to the result in mass-imbalanced HM in Refs. 9 and 23.

It is to be noticed that in the half-filled band case, due to a particle-hole symmetry $\rho_{\sigma\alpha}(\omega) = \rho_{\sigma\alpha}(-\omega)$, from Eq. (4), it is clear that the real part of Green functions

at the Fermi level ($\omega = 0$) is zero, i.e. $G_\sigma(0) = -i\pi\rho_{\sigma\alpha}(0)$. Then it is not difficult to find the averaged LDOS at the Fermi level, which indicates the ground state properties of the system, from numerical solving Eqs. (5) and (6), if the atomic limit for $\langle n_i\rangle$ is used

$$\langle n_i\rangle = \begin{cases} 2 & \text{if } \varepsilon_i < -U/2, \\ 1 & \text{if } -U/2 < \varepsilon_i < U/2, \\ 0 & \text{if } \varepsilon_i > U/2. \end{cases} \tag{7}$$

Next, taking into account that on the metallic side the LDOS is arbitrarily small in the vicinity of the MIT region,[12,16] the linearized DMFT equations determining the MIT for both geometrical and arithmetical mean can be obtained. A pair of linear equations for $\rho_{\uparrow a}(0), \rho_{\downarrow a}(0)$ takes the form

$$[t_\uparrow^2 I_1(U,\Delta) - 1]\rho_{\uparrow a}(0) + UI_2(U,\Delta)t_\downarrow^2\rho_{\downarrow a}(0) = 0, \tag{8}$$

$$UI_2(U,\Delta)t_\uparrow^2\rho_{\uparrow a}(0) + [t_\downarrow^2 I_1(U,\Delta) - 1]\rho_{\downarrow a}(0) = 0, \tag{9}$$

where

$$I_1(U,\Delta) = \frac{1}{\Delta}\int_{-\Delta/2}^{\Delta/2} \frac{\varepsilon^2 + U^2/4 + (1-n_i)U\varepsilon}{[\varepsilon^2 - U^2/4]^2} d\varepsilon, \tag{10}$$

$$I_2(U,\Delta) = \frac{1}{\Delta}\int_{-\Delta/2}^{\Delta/2} \frac{U/2 + (1-n_i)\varepsilon}{[\varepsilon^2 - U^2/4]^2} d\varepsilon. \tag{11}$$

The system of linear equations (8) and (9) has a nonzero values of $\rho_{\sigma a}(0)$ if and only if their determinant vanishes, giving the linearized DMFT equation with arithmetical mean ($t_\uparrow = 1$ sets the energy unit)

$$[I_1(U,\Delta) - 1][r^2 I_1(U,\Delta) - 1] - [UrI_2(U,\Delta)]^2 = 0. \tag{12}$$

We note that in the limit cases $r = 0$ and $r = 1$ Eq. (12) is reduced to Eq. (15) in Ref. 12 and Eq. (13) in Ref. 16, correspondingly.

A pair of equations for $\rho_{\uparrow g}(0), \rho_{\downarrow g}(0)$ is also obtained

$$\rho_{\uparrow g}(0) = \exp\left[\frac{1}{\Delta}\int_{-\Delta/2}^{\Delta/2} \ln\left(\frac{t_\uparrow^2(\varepsilon^2 + U^2/4 + (1-n_i)U\varepsilon)\rho_{\uparrow g}(0)}{[\varepsilon^2 - U^2/4]^2} + \frac{Ut_\downarrow^2(U/2 + (1-n_i)\varepsilon)\rho_{\downarrow g}(0)}{[\varepsilon^2 - U^2/4]^2}\right) d\varepsilon\right], \tag{13}$$

$$\rho_{\downarrow g}(0) = \exp\left[\frac{1}{\Delta}\int_{-\Delta/2}^{\Delta/2} \ln\left(\frac{Ut_\uparrow^2(U/2 + (1-n_i)\varepsilon)\rho_{\uparrow g}(0)}{[\varepsilon^2 - U^2/4]^2} + \frac{t_\downarrow^2(\varepsilon^2 + U^2/4 + (1-n_i)U\varepsilon)\rho_{\downarrow g}(0)}{[\varepsilon^2 - U^2/4]^2}\right) d\varepsilon\right]. \tag{14}$$

Again, in the limit cases $r = 0$ and $r = 1$ Eqs. (13) and (14) is reduced to Eq. (14) in Ref. 12 and Eq. (11) in Ref. 16, correspondingly. However, for $0 < r < 1$, they

do not yield an equation determining the curve border $\Delta = \Delta(U)$ for the Anderson MIT like Eq. (12) for the Mott MIT. On the other hand, it follows readily from the above linearized DMFT equations (8) and (9) for $\rho_{\uparrow a}(0), \rho_{\downarrow a}(0)$ as well as those (13) and (14) for $\rho_{\uparrow g}(0), \rho_{\downarrow g}(0)$ that both $\rho_{\sigma a}(0)$ simultaneously vanish at the critical value of interaction and disorder, so do both $\rho_{\sigma g}(0)$. These critical values for $\rho_{\sigma a}(0)$ and $\rho_{\sigma g}(0)$, as shown in the following section, are almost the same only for small disorder. In addition, one can easily verify that in the non-interacting case $U = 0$ each spin component is localized by the different values of critical disorder strength.

3. Results and Discussion

In this section, we turn to present and discuss our numerical results with $t_\uparrow = 1$ as the energy unit. In the TMT, the vanishing of arithmetically averaged LDOS $\rho_{\sigma a}(0)$ indicates a Mott transition (from gapless phase to gapped phase) while the vanishing of geometrically averaged LDOS $\rho_{\sigma g}(0)$ signalizes an Anderson transition (from extended gapless phase to localized gapless phase) for particles with spin σ. Figure 1 shows geometrically and arithmetically averaged LDOS in the band center ($\omega = 0$) with $r = 0.5, \Delta = 1.0$ (upper panel) and $\Delta = 4.0$ (lower panel) as a function of U. One can see that both $\rho_{\sigma a}(0)$ as well as $\rho_{\sigma g}(0)$ simultaneously vanish at the phase transition as predicted by the linearized DMFT equations. It is well established that in the mass imbalanced HM both spin components localize simultaneously at the critical interaction value.[7–10] Here, we show that in the presence of disorder, this property is still preserved in the system. Furthermore, at small value of disorder $\Delta(\Delta = 1)$, increasing U leads to a decreasing of the averaged LDOS at

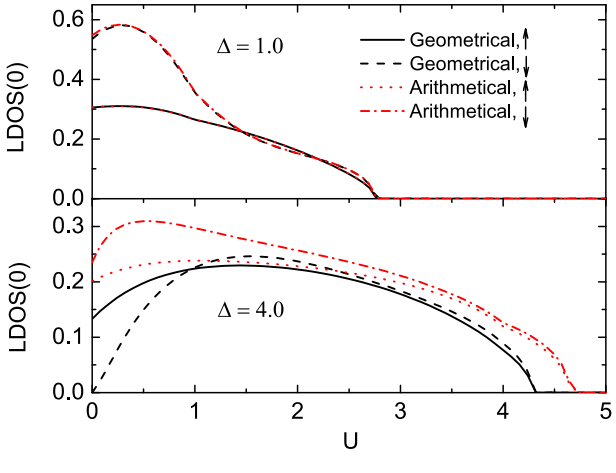

Fig. 1. (Color online) Geometrically and arithmetically averaged LDOS for both spin components in the band center ($\omega = 0$) with $r = 0.5, \Delta = 1.0$ (upper panel) and $\Delta = 4.0$ (lower panel) as a function of U. Solid (dot) lines are determined by using geometrical (arithmetical) averaging for up-spin component. Dash (dash dot) lines are determined by using geometrical (arithmetical) averaging for down-spin component. Energy parameters U, Δ are in the unit set by $t_\uparrow = 1$.

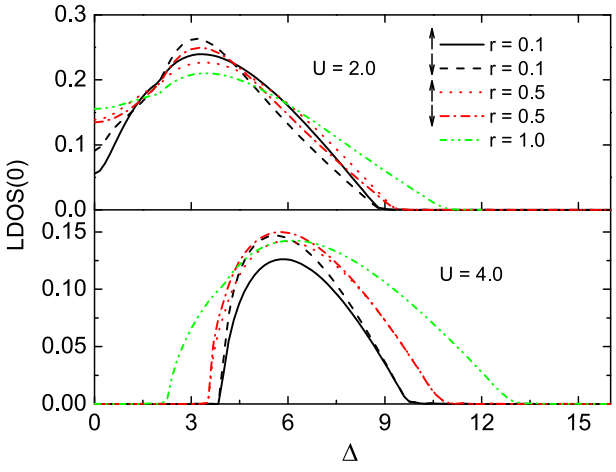

Fig. 2. (Color online) Geometrically averaged LDOS in the band center ($\omega = 0$) with $r = 0.1, 0.5, 1.0$ for $U = 2.0$ (upper panel) and for $U = 4.0$ (lower panel) as a function of Δ. Solid (dash) lines are calculated for $r = 0.1$ for up-spin (down-spin) components. Dot (dash dot) lines are calculated for $r = 0.5$ for up-spin (down-spin) components. Dash-dot-dotted line is calculated for the balanced case $r = 1$.

the band center for both spin components, and both averaging over the disorder give almost the same result for the value of critical interaction. It means that at small Δ the direct metal–Mott insulator transition is found. On the other hand, at larger $\Delta(\Delta = 4)$, the behavior of the averaged LDOS is more complicated, $\rho_{\sigma g}(0)$ goes to zero at a smaller value of U than does $\rho_{\sigma a}(0)$, that means direct metal–Anderson insulator transition is found. In addition, it can be seen from lower panel that for $U = 0$ the geometric LDOS(0) for spin-down is equal to zero, while the one for spin-up is finite, therefore for $U = 0, \Delta = 4$ the system is partially localized. A detailed discussion of this novel phase will be given later.

In Fig. 2, we present geometrically averaged LDOS in the band center ($\omega = 0$) with $r = 0.1, 0.5, 1.0$ for $U = 2.0$ (upper panel) and for $U = 4.0$ (lower panel) as a function of Δ. In the upper panel, they all have a similar behavior with increasing disorder strength: increase to their maximal values, then decrease to zero at critical disorder strengths Δ_c. Again, for a fixed mass imbalance parameter $\rho_{\sigma g}(0)$ for both spin components simultaneously vanish at the same Δ_c, however this value increases with increasing r. This implies that for a fixed r and small U a single Anderson MIT occurs when the disorder strength reaches its critical value. The behavior of $\rho_{\sigma g}(0)$ in lower panel differs from those in former case that when the disorder is increased the Anderson MIT occurs twice: At the critical strength Δ_{c1} the system undergoes from the Anderson insulator to the metal, i.e. the disorder stabilizes the metallic phase, and at larger Δ_{c2} from the metal to the Anderson insulator. One can see that with increasing the mass imbalance (r decreases) Δ_{c1} increases, while Δ_{c2} decreases, i.e. the Anderson insulator region is enlarged.

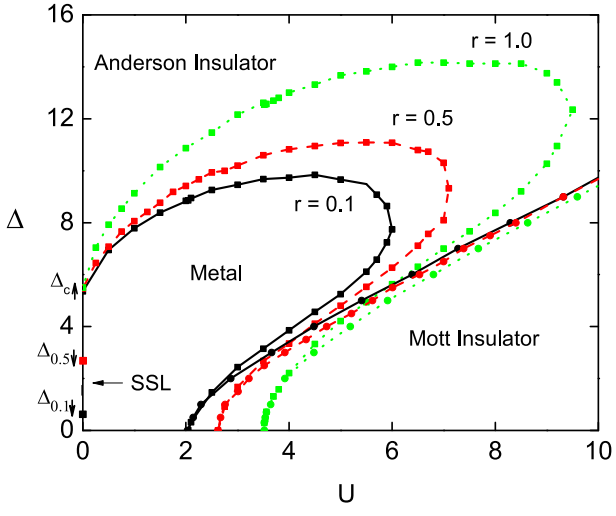

Fig. 3. (Color online) Nonmagnetic ground state phase diagram for the half-filled AHM with mass imbalance for different values of $r = 0.1, 0.5$ and comparison with the result of the balanced case $r = 1$. Solid with squares (solid with dots) lines are determined by using geometrical (arithmetical) averaging for $r = 0.1$. Dash with squares (dash with dots) lines are determined by using geometrical (arithmetical) averaging for $r = 0.5$. Dot with squares (dot with dots) lines are determined by using geometrical (arithmetical) averaging for the balanced case $r = 1$. The spin-selective localized phase is located in the line $U = 0, \Delta_{r\downarrow} < \Delta < \Delta_{c\uparrow}$.

The main result of our investigation is the nonmagnetic ground state phase diagram of the mass imbalanced AHM at half-filling shown in Fig. 3 for different values of $r = 0.1, 0.5$, and 1. Our result in the mass imbalanced limit $r = 0$ (not shown here) is recovered the AFKM in Ref. 12, while those of the mass balanced case $r = 1$ is presented for the comparison. For $0 < r < 1$ four different phases are observed in the phase diagram: (1) The Anderson insulator phase is defined by $\rho_{\sigma g}(0) = 0, \rho_{\sigma a}(0) > 0$. In the non-interacting system, the critical disorder strength $\Delta_{c\uparrow}(U = 0) = 2e$ for all r. Similar to the mass balanced case, here, larger Δ favors the Anderson localization. In addition, the Anderson insulator region is enlarged with increasing the mass imbalance (r decreases) because at fixed $t_\uparrow$ the larger the difference in the bare mass, the smaller $t_\downarrow$ and the easier it is to localize the system. (2) The Mott insulator phase is identified by $\rho_{\sigma a}(0) = 0$. In the non-disordered system, the critical interaction can be analytically found from the linearized DMFT equations: $U_c(\Delta = 0, r) = [2(1 + r^2 + \sqrt{1 + 14r^2 + r^4})]^{1/2}$, i.e. a monotonically increasing function of r, and $U_c(\Delta = 0, r = 0) = 2; U_c(\Delta = 0, r = 1) = 2\sqrt{3}$ as in AFKM[12] and AHM,[16] keeping in mind that in Refs. 12 and 16 $W = 4t_\uparrow$ is the energy unit. As in the balanced case the Mott insulator stabilizes with increasing U. Furthermore, its region is enlarged with increasing the mass imbalance (r decreases) for the same reason as the Anderson insulator. (3) The metal is determined by $\rho_{\sigma g}(0) > 0$ and found for small values of U and Δ. Its shape is similar to those

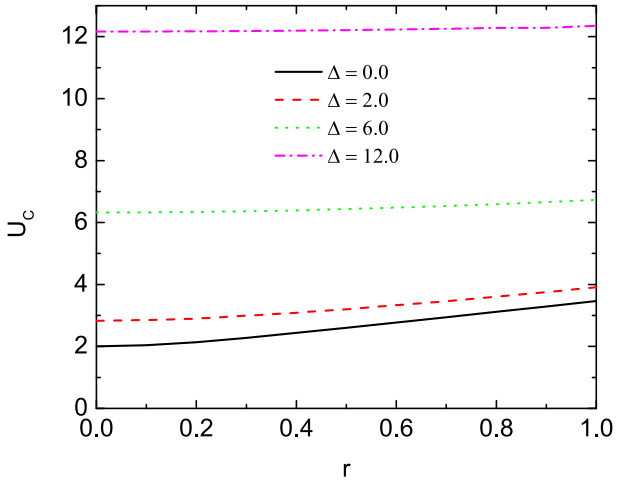

Fig. 4. (Color online) The critical interaction U_c determining the Mott MIT as a monotonically increasing function of r for various values of $\Delta = 0, 2, 6$, and 12. It is clearly seen that the difference between $U_c(1)$ and $U_c(0)$ decreases with increasing Δ.

of the balanced case, but its region is reduced with increasing the mass imbalance (r decreases) because the region of both types of insulator are enlarged. (4) The partially localized or spin-selective localized phase, where the spin-down particles are localized ($\rho_{\downarrow g}(0) = 0$) while those with spin-up are still itinerant ($\rho_{\uparrow g}(0) > 0$). This phase originates from the mass imbalance in the system and takes place when $U = 0$ and $2er = \Delta_{r\downarrow}(U = 0) < \Delta < \Delta_{c\uparrow}(U = 0) = 2e$. It should be noted that without interaction ($U = 0$) the two spin components are independent, and the spin-selective localized phase can be found, but as soon as the interaction is switched on the two spin components are coupled, as a result $\rho_{\uparrow g}(0), \rho_{\downarrow g}(0)$ are vanished simultaneously and the spin-selective localized phase no longer exists. This is the correlation effect because the suppression of the double occupation of the two spin components in the insulating state must be satisfied simultaneously.

In Fig. 4, we plot U_c as a function of r for various values of $\Delta = 0, 2, 6$, and 12. It is well established that in the mass imbalanced HM ($\Delta = 0$) the critical interaction U_c is a monotonically increasing function of r.[7–10] It is clearly seen from Fig. 4 that U_c increases when Δ increases and for a finite and fixed ΔU_c is still a monotonically increasing function of r. However with increasing Δ the difference between $U_c(1)$ and $U_c(0)$ decreases, and for larger $\Delta(\Delta > 12)$ we find $U_c(r)$ tends to Δ for all r. It means that within our approximation for large Δ, the boundary between two types of insulators in the mass imbalanced system occurs at $U \approx \Delta$ as in the mass balanced one in Refs. 13 and 16. However, this contradicts the more accurate result for the AFKM in Ref. 12, where the border between these two types of insulators $\Delta(U) \approx 2e\sqrt{2}$ was estimated for $r = 0$ and $U \gg 4$. It can be explained by the fact that our used approximation is better suited for small values of U and Δ.

4. Conclusions

We have studied the ground state phase diagram of the mass imbalanced AHM at half-filling by using the DMFT with the geometrical average over the disorder and the EOM as an impurity solver. In addition to the three phases that showed up in the balanced case, the phase diagram of the mass imbalanced case contains a spin-selective localized phase. Note that origin of the spin-selective localized phase is not unique, it originates from the mass imbalance in this study and from the spin-dependent disorder in Refs. 19 and 20. We have discussed the nonmagnetic ground state properties of the system for various values of the mass imbalance parameter r. In the limit cases $r = 0, 1$ our results recover those of the AFKM in Ref. 12 and the AHM in Ref. 16, correspondingly. For $0 < r < 1$ we found that excluding the non-interacting case the phase transition occurs simultaneously for two spin components, both the Anderson and Mott insulator region are enlarged and the metallic one is reduced as the mass imbalance increased. The phase diagram of the mass imbalanced AHM also differs from those of the balanced case by the fact that the spin-selective localized phase is appeared in the line $U = 0, \Delta_{r\downarrow} < \Delta < \Delta_{c\uparrow}$. For a fixed Δ the Mott critical interaction increases when the mass imbalance decreases, and for larger Δ both types of insulator are connected. In our study at zero temperature, all phase transitions are continuous.

The experiment test of our prediction can be performed when the ultracold atom mixture, for example the ^{6}Li^{40}K, is loaded in the disordered optical lattices.

Acknowledgments

This research is funded by the National Foundation for Science and Technology Development (NAFOSTED) under Grant No. 103.01-2020.20. The partially final support through ICP.2020.01 of the International Center of Physics at the Institute of Physics, Vietnam Academy of Science and Technology is acknowledged.

References

1. Q. Chen, J. Stajic, S. Tan and K. Levin, *Phys. Rep.* **412** (2008) 1.
2. R. Jordens *et al.*, *Nature* **455** (2008) 204.
3. S. S. Kondov *et al.*, *Science* **334** (2011) 66.
4. M. V. Zwierlein, A. Schirotzek, C. H. Schunck and W. Ketterle, *Science* **311** (2006) 492.
5. E. Wille *et al.*, *Phys. Rev. Lett.* **100** (2008) 053201.
6. M. Taglieber *et al.*, *Phys. Rev. Lett.* **100** (2008) 010401.
7. E. A. Winograd, R. Chitra and M. J. Rozenberg, *Phys. Rev. B* **84** (2011) 233102.
8. T. L. Dao, M. Ferrero, P. S. Cornaglia and M. Capone, *Phys. Rev. A* **85** (2012) 013606.
9. A. T. Hoang, T. T. T. Tran and D. A. Le, *J. Korean Phys. Soc.* **68** (2016) 238.
10. A. T. Hoang and D. A. Le, *Physica B* **485** (2016) 121.
11. V. Dobrosavljevic, A. A. Pastor and B. K. Nikolic, *Europhys. Lett.* **62** (2003) 76.
12. K. Byczuk, *Phys. Rev. B* **71** (2005) 205105.

13. M. C. O. Aguiar, V. Dobrosavljevic, E. Abrahams and G. Kotliar, *Phys. Rev. Lett.* **102** (2009) 156402.
14. K. Byczuk, W. Hofstetter and D. Vollhardt, *Int. J. Mod. Phys. B* **24** (2010) 1727.
15. D. Semmler *et al.*, *Phys. Rev. B* **84** (2011) 115113.
16. A. T. Hoang, T. H. Y. Nguyen and D. A. Le, *Physica B* **570** (2019) 320.
17. K. Byczuk, W. Hofstetter and D. Vollhardt, *Phys. Rev. Lett.* **94** (2005) 0564021.
18. W. S. Oliveira, M. C. O. Aguiar and V. Dobrosavljevic, *Phys. Rev. B* **89** (2014) 165138.
19. J. Skolimowski, D. Vollhardt and K. Byczuk, *Phys. Rev. B* **92** (2015) 09402.
20. J. Skolimowski *et al.*, *J. Phys. Commun.* **2** (2018) 025031.
21. Q. Feng, Study of single impurity Anderson model and dynamical mean field theory based on equation of motion method, Ph.D. thesis, Goethe Universitat Frankfurt, Frankfurt am Main, Germany (2009).
22. A. Georges *et al.*, *Rev. Mod. Phys.* **68** (1996) 13.
23. I. V. Stasyuk and O. B. Hera, *Eur. Phys. J. B* **48** (2005) 339.